Solution ^{1}H, ^{15}N NMR Spectroscopic Characterization of Substrate-Bound, Cyanide-Inhibited Human Heme Oxygenase: Water Occupation of the Distal Cavity

Yiming Li,[†] Ray T. Syvitski,[†] Karine Auclair,[‡,§] Paul Ortiz de Montellano,[‡] and Gerd N. La Mar[†,*]

Contribution from the Department of Chemistry, University of California, Davis, California 95616 and Department of Pharmaceutical Chemistry, University of California, San Francisco, California 94143-2280

Received May 15, 2003; E-mail: lamar@indigo.ucdavis.edu

Abstract: A solution NMR spectroscopic study of the cyanide-inhibited, substrate-bound complex of uniformly ^{15}N-labeled human heme oxygenase, hHO, has led to characterization of the active site with respect to the nature and identity of strong hydrogen bonds and the occupation of ordered water molecules within both the hydrogen bonding network and an aromatic cluster on the distal side. {^{1}H−^{15}N}-HSQC spectra confirm the functionalities of several key donors in particularly robust H-bonds, and {^{1}H−^{15}N}HSQC-NOESY spectra lead to the identification of three additional robust H-bonds, as well as the detection of two more relatively strong H-bonds whose identities could not be established. The 3D NMR experiments provided only a modest, but important, extension of assignments because of the loss of key TOCSY cross-peaks due to the line broadening from a dynamic heterogeneity in the active site. Steady-state NOEs upon saturating the water signal locate nine ordered water molecules in the immediate vicinity of the H-bond donors, six of which are readily identified in the crystal structure. The additional three are positioned in available spaces to account for the observed NOEs. ^{15}N-filtered steady-state NOEs upon saturating the water resonances and ^{15}N-filtered NOESY spectra demonstrate significant negative NOEs between water molecules and the protons of five aromatic rings. Many of the NOEs can be rationalized by water molecules located in the crystal structure, but strong water NOEs, particularly to the rings of Phe47 and Trp96, demand the presence of at least an additional two immobilized water molecules near these rings. The H-bond network appears to function to order water molecules to provide stabilization for the hydroperoxy intermediate and to serve as a conduit to the active site for the nine protons required per HO turnover.

Introduction

The nonmetal enzyme heme oxygenase, HO,[1] carries out the highly stereoselective cleavage of hemin into biliverdin-IXα, iron, and CO, utilizing three O_2 molecules, seven electrons, and nine protons, with hemin serving as both cofactor and substrate.[2−5] In mammals, HO occurs as three ∼32 kDa membrane-bound enzymes whose role is to catabolize hemin and conserve iron[6] (HO-1) or generate CO (HO-2) as a putative neural messenger;[7] the function of the third isoform is yet to be established.[8] Shorter (∼210 residue), soluble HOs have been characterized in pathogenic bacteria such as *C. diphtheriae* (named HmuO)[9,10] and *N. meningitidis* (named HemO),[11,12] where their function appears to be to "mine" iron from the host's heme. A soluble ∼200 residue HO occurs in plants and cyanobacteria where it functions to generate open tetrapyrroles as light harvesting antennae.[13] The reaction of HO appears common for the diverse sources of the enzyme and is characterized by a ferric hydroperoxy intermediate, rather than the $Fe^{IV}=O$ group of cytochromes P450, as the source of the oxygen inserted into the C−H bond in the first step in which the α-meso position is hydroxylated.[3−5,14]

[†] University of California, Davis.

[‡] University of California, San Francisco.

[§] Present Address: Department of Chemistry, McGill University, 801 Sherbrooke Street West, H3A 2K6 Montreal, Quebec, Canada.

(1) Abbreviations used: HO, heme oxygenase; hHO, human heme oxygenase; rHO, rat heme oxygenase; HmuO, *C. diphtheriae* heme oxygenase; DMDH, 2,4-dimethyldeutrohemin; PH, protohemin; HSQC, heteronuclear single quantum coherence; NOE, nuclear Overhauser effect; NOESY, 2D nuclear Overhauser spectroscopy; TOCSY, 2D total correlation spectroscopy; DSS, 2,2-dimethyl-2-silapentane-5-sulfonate; FID, free-induction decay; TROSY, transverse relaxation-optimized spectroscopy.

(2) Tenhunen, R.; Marver, H. S.; Schmid, R. *J. Biol. Chem.* **1969**, *244*, 6388−6394.

(3) Ortiz de Montellano, P. R. *Curr. Opin. Chem. Biol.* **2000**, *4*, 221−227.

(4) Ortiz de Montellano, P. R.; Auclair, K. In *The Porphyrin Handbook*; Kadish, K. M., Smith, K. M., Guilard, R., Eds.; Elsevier Science: San Diego, CA, 2003; Vol. 12, pp 175−202.

(5) Yoshida, T.; Migita, C. T. *J. Inorg. Biochem.* **2000**, *82*, 33−41.

(6) Yoshida, T.; Biro, P.; Cohen, T.; Mueller, R. M.; Shibahara, S. *Eur. J. Biochem.* **1988**, *171*, 457−461.

(7) Maines, M. D. *Annu. Rev. Pharmacol. Toxicol.* **1997**, *37*, 517−554.

(8) McCoubrey, W. K.; Huang, T. J.; Maines, M. D. *Eur. J. Biochem.* **1997**, *247*, 725−732.

(9) Schmitt, M. P. *J. Bacteriol.* **1997**, *179*, 838−845.

(10) Chu, G. C.; Katakura, K.; Zhang, X.; Yoshida, T.; Ikeda-Saito, M. *J. Biol. Chem.* **1999**, *274*, 21319−21325.

(11) Zhu, W.; Willks, A.; Stojiljkovic, I. *J. Bacteriol.* **2000**, *182*, 6783−6790.

(12) Wilks, A.; Schmitt, M. P. *J. Biol. Chem.* **1998**, *273*, 837−841.

(13) Beale, S. I. In *The molecular biology of cyanobacteria*; Bryant, D. A., Ed.; Academic Publishers: Dordrecht, 1994; pp 519−558.

(14) Davydov, R.; Kofman, V.; Fujii, H.; Yoshida, T.; Ikeda-Saito, M.; Hoffman, B. M. *J. Am. Chem. Soc.* **2002**, *124*, 1798−1808.
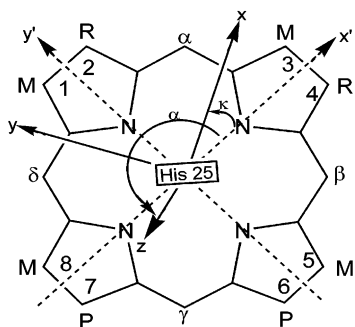
Figure 1. Structures and numbering of native protohemin, PH, with R = vinyl, and 2-fold symmetric 2,4-dimethyldeuterohemin, DMDH, with R = methyl. The iron-centered reference frame, x', y', z', and the previously reported magnetic axes, x, y, z are shown, where the tilt of the major magnetic (z) axis from the heme normal (z'-axis) is given by the angle β, and its direction of tilt is defined by α, the angle between the projection z on the z',y'-plane are the x' axis. The rhombic axes are located by κ, the angle between the projection of the x,y-axis onto the heme plane and the x'-axis.

Crystal structures of truncated, soluble, but fully active mammalian substrate complexes of HO (human HO, hHO,[15−17] rat HO, rHO[18,19]), followed by those of bacterial HOs,[20,21] have revealed homologous, essentially α-helical enzymes where the α-meso stereoselectivity is, in large part, rationalized by the placement of the distal helix so close to the heme as to sterically impede access of the hydroperoxy ligand to all but the α-meso position. A second, distinct steric contribution to stereoselectivity was proposed based on resonance Raman[22] and NMR[23−25] data that indicated steric tilting of the axial ligand toward the α-meso position. More recent crystal structures of the azide complex of substrate-bound rHO, rHO−PH−N$_3$[19] (PH = protohemin, R = vinyl in Figure 1) and the NO complex of substrate-bound, reduced hHO[26] confirm this proposal. The mechanism by which a ferric hydroperoxy intermediate is stabilized relative to the more common ferryl unit was initially unclear in the crystal structure.[15] Moreover, the initial structure did not reveal the nature of the distal residue which exhibited a titratable proton[27−29] and induced an isotope effect in the EPR spectrum of the oxy complex of the Co(II) substituted substrate complex of rHO.[30]

Last, unusually large voids were located in the distal pocket of both the hHO and rHO substrate complexes.[15,18] The observation that mutating the conserved Asp140 on the distal helix, which is too distant to directly exercise any influence on the iron ligand, abolishes oxygenase activity,[16,31] together with the crystallographic location of ordered water molecules near the key Asp140 carboxylate,[16] suggested that water molecules may provide the link between substrate ligand and the Asp140. Again, such a solvent linked H-bond is observed in the rHO−PH−N$_3$ and reduced hHO−PH−NO crystal structures.[19,26]

^{1}H NMR investigations of substrate-bound, cyanide-inhibited complexes of both hHO[25] and HmuO[32] have revealed the presence of H-bonding networks that extend from the distal pocket to the opposite side of the enzyme. The H-bond network is not obvious in either crystal structure,[15,21] but the crystal structures readily identify the acceptors that account for the unusually strong H-bonds (NH, OH chemical shifts 10−18 ppm[33]) whose donors are uniquely identified by ^{1}H NMR. These strong H-bond donor protons, moreover, exhibit[34] sizable NOEs due to the presence of "ordered" water molecules in their immediate vicinity[35] (<3 Å), not all of which are apparent in the crystal structure.[15,17] The large, negative NOEs of strong H-bond donor protons to immobilized water molecules of the substrate complexes of *C. diphtheria* heme oxygenase, HmuO, have shown[32] that the H-bonding network and ordered water molecules are conserved in the HmuO substrate complex.[32] A water channel is readily observed in the HmuO crystal structure.[21]

It is thus apparent that organized water molecules are present in HO complexes in larger numbers than in other metalloenzymes in general,[36,37] but heme enzymes in particular,[36] and it is likely that such water molecules play key roles in various aspects of the reaction mechanism characteristic of HO.[3−5] Solution ^{1}H NMR, under appropriate conditions, is well suited to the detection of organized water molecules.[35] While the lifetimes of such ordered water molecules within the enzyme are too short (<1 ms) to detect signals resolved from the bulk water, the presence of such water molecules can be inferred from the observation of NOEs between bulk water and protons of the enzyme, provided it can be demonstrated that the NOE cannot arise from a labile proton in the enzyme which, itself, exchanges rapidly with bulk water.[35] The sign of the NOE sets lower limits on the residence time of the water molecules and the NOE magnitude allows placement, upon modeling, of the water molecule within the molecular framework. Seven water molecules, and a likely eighth, were so identified[34] for the hHO−DMDH−CN complex (DMDH = 2,4-dimethyldeuterohemin, R = methyl in Figure 1, a 2-fold symmetric substrate[38] that obviates the adverse influences on resolution of heme

(15) Schuller, D. J.; Wilks, A.; Ortiz de Montellano, P. R.; Poulos, T. L. *Nat. Struct. Biol.* **1999**, *6*, 860−867.
(16) Koenigs Lightning, L.; Huang, H.-W.; Moënne-Loccoz, P.; Loehr, T. M.; Schuller, D. J.; Poulos, T. L.; Ortiz de Montellano, P. R. *J. Biol. Chem.* **2001**, *276*, 10612−10619.
(17) Lad, L.; Schuller, D. J.; Shimizu, H.; Friedman, J.; Li, H.; Ortiz de Montellano, P. R.; Poulos, T. L. *J. Biol. Chem.* **2003**, *278*, 7834−7843.
(18) Sugishima, M.; Omata, Y.; Kakuta, Y.; Sakamoto, H.; Noguchi, M.; Fukuyama, K. *FEBS Lett.* **2000**, *471*, 61−66.
(19) Sugishima, M.; Sakamoto, H.; Higashimoto, Y.; Omata, Y.; Hayashi, S.; Noguchi, M.; Fukuyama, K. *J. Biol. Chem.* **2002**, *45086*−45090.
(20) Schuller, D. J.; Zhu, W.; Stojiljkovic, I.; Wilks, A.; Poulos, T. L. *Biochemistry* **2001**, *40*, 11552−11558.
(21) Hirotsu, S.; Chu, G. C.; Lee, D.-S.; Unno, M.; Yoshida, T.; Park, S.-Y.; Shiro, Y. S.; Ikeda-Saito, M. *Protein Data Bank (accession number of 1WI0)*, manuscript in preparation.
(22) Takahashi, S.; Ishikawa, K.; Takeuchi, N.; Ikeda-Saito, M.; Yoshida, T.; Rousseau, D. L. *J. Am. Chem. Soc.* **1995**, *117*, 6002−6006.
(23) Gorst, C. M.; Wilks, A.; Yeh, D. C.; Ortiz de Montellano, P. R.; La Mar, G. N. *J. Am. Chem. Soc.* **1998**, *120*, 8875−8884.
(24) La Mar, G. N.; Asokan, A.; Espiritu, B.; Yeh, D. C.; Auclair, K.; Ortiz de Montellano, P. R. *J. Biol. Chem.* **2001**, *276*, 15676−15687.
(25) Li, Y.; Syvitski, R. T.; Auclair, K.; Wilks, A.; Ortiz de Montellano, P. R.; La Mar, G. N. *J. Biol. Chem.* **2002**, *277*, 33018−33031.
(26) Lad, L.; Wang, J.; Li, H.; Friedman, J.; Bhaskar, B.; Ortiz de Montellano, P. R.; Poulos, T. L. *J. Mol. Biol.* **2003**, *330*, 527−538.
(27) Sun, J.; Wilks, A.; Ortiz de Montellano, P. R.; Loehr, T. M. *Biochemistry* **1993**, *32*, 14151−14157.
(28) Takahashi, S.; Wang, J.; Rousseau, D. L.; Ishikawa, K.; Yoshida, T.; Host, J. R.; Ikeda-Saito, M. *J. Biol. Chem.* **1994**, *269*, 1010−1014.
(29) Takahashi, S.; Wang, J. L.; Rousseau, D. L.; Ishikawa, K.; Yoshida, T.; Takeuchi, N.; Ikeda-Saito, M. *Biochemistry* **1994**, *33*, 5531−5538.
(30) Fujii, H.; Dou, Y.; Zhou, H.; Yoshida, T.; Ikeda-Saito, M. *J. Am. Chem. Soc.* **1998**, *120*, 8251−8252.
(31) Fujii, H.; Zhang, X.; Tomita, T.; Ikeda-Saito, M.; Yoshida, T. *J. Am. Chem. Soc.* **2001**, *123*, 6475−6484.
(32) Li, Y.; Syvitski, R. T.; Chu, G. C.; Ikeda-Saito, M.; La Mar, G. N. *J. Biol. Chem.* **2003**, *279*, 6651−6663.
(33) Harris, T. K.; Mildvan, A. S. *Proteins*: *Struct., Funct., Genet.* **1999**, *35*, 275−282.
(34) Syvitski, R. T.; Li, Y.; Auclair, K.; Ortiz de Montellano, P. R.; La Mar, G. N. *J. Am. Chem. Soc.* **2002**, *124*, 14296−14297.
(35) Otting, G. *Prog. NMR Spectrosc.* **1997**, *31*, 259−285.
(36) Messerschmidt, A., Huber, R., Poulos, T. L., Wieghardt, K., Eds. *Handbook of Metalloproteins*; Wiley & Sons, Ltd.: Chichester, UK, 2001; Vol. 1.
(37) Messerschmidt, A., Huber, R., Poulos, T. L. Wieghardt, K., Eds. *Handbook of Metalloproteins*; Wiley & Sons, Ltd.: Chichester, UK, 2001; Vol. 2.
(38) Tomaro, M. L.; Frydman, S. B.; Frydman, B.; Pandey, R. K.; Smith, K. M. *Biochim. Biophys. Acta* **1984**, *791*, 342−349.

orientational disorder about the $\alpha-\gamma$-meso axis), because the strong H-bond donor protons exhibited resolved resonances that could be sequence-specifically assigned,[25] and it was demonstrated[34] that the exchange rates with bulk water for seven of these labile protons were much too slow to have chemical exchange contributions to the observed magnetization transfer.

An intriguing observation for hHO−DMDH−CN[34] was an NOE between bulk water and a ring proton of Phe95. This was the only water NOE attributed to an aromatic ring, because Phe95 is one of only two aromatic rings (the other is Trp101) which exhibited a nonlabile ring resonance resolved from the intense 8−6 ppm envelope of NH, OH, and other aromatic ring protons.[25] NOEs or NOESY cross-peaks between the water resonance and other aromatic ring protons are hopelessly obscured by the spectral congestion and magnetization transfer via chemical exchange to the more labile NHs and OHs in the same spectral window. To extend the NMR characterization of water access to aromatic residues in the active site of HO, we report herein on our initial NMR study of a uniformly ^{15}N-enriched hHO−PH−CN complex which, while providing only a modest increase in the number of assigned residues in hHO−PH−CN relative to those achieved solely by ^{1}H 2D NMR on hHO−DMDH−CN,[25] provides crucial confirmation for the proposed functionality of several strong H-bond donors and allows the demonstration that a series of water molecules are localized near numerous interacting aromatic rings in the distal pocket.

Experimental Methods

Materials. The QuickChange site-directed mutagenesis kit and the nitrilotriacetic acid resin (NTA-Agarose) were obtained from Stratagene (La Jolla, CA). The nickel columns were generated by washing the NTA resin with 5 column volumes of 100 mM nickel sulfate. NADH, NADPH, EDTA, potassium phosphate, hemin, leupeptin, chymostatin, pepstatin A, PMSF, H_2O_2, guaiacol, dithiothreitol, sodium dithionite, β-mercaptoethanol, and DEAE Sepharose were purchased from Aldrich or Sigma. Yeast extract, tryptone, 2YT, sodium chloride, imidazole, EDTA, and organic solvents were obtained from Fisher Scientific (Fair Lawn, NJ). Isopropyl-β-D-thiogalactopyranoside was from FisherBiotech (Fair Lawn, NJ), and ampicillin, from Promega (Madison, WI). Q-Sepharose and 2′,5′-ADP-Sepharose were from Amersham Pharmacia Biotech (Sweden). The hydroxyapatite gel (Bio-Gel HTP Gel) was obtained from Bio-Rad Laboratories (Hercules, CA). High purity argon (99.998%), CO (99.9%), and the oxygen adsorbent, Oxisorb-W, used to further purify the argon were purchased from Puritan-Bennett Medical Gases (Overland Park, KS). All the chemicals were used without further purification. HPLC was performed on a Hewlett-Packard 1090 liquid chromatograph. The UV−visible spectra were recorded on a Hewlett-Packard 8452A diode array spectrophotometer or on a Cary 1E Varian UV−visible spectrophotometer.

Preparation of the Expression Plasmid hHO in pcWori. Truncated human heme oxygenase-1 (hHO, residues 1−265, designated hHO) is routinely expressed in our laboratories using the pBAce vector,[39] but this expression system is not compatible with the use of a minimal media. It was therefore suitable to test other expression systems. Among the several vectors tested, pcWori showed the best expression level and protein stability in either complete or minimal media. To prepare this expression system, a pcWori vector containing the P450cam insert and the plasmid of hHO in the pBAce vector were separately digested with the restriction enzymes NdeI and XbaI. The hHO gene was then ligated into pcWori.

Expression of ^{15}N-hHO. The levels of expression were determined for two different types of cells (DH5α and BL21(DE3)pLys) in complete media (LB or 2YT) as well as in minimal media (AMM, M9) grown at 25 or 37 °C overnight, after induction with IPTG (0.1, 0.5, or 1 mM, at $OD_{600} \approx 0.8$) and with or without addition of δ-aminolevulinic acid (400 nM). Based on the color of the cells and on SDS-PAGE of the cell pellets, the expression of hHO was found to be negligible in DH5α cells but comparable to the standard expression conditions[39] when BL21(DE3)pLys cells were used. The optimum conditions included the use of LB or AMM media, 0.5 mM IPTG, 400 nM δ-aminolevulinic acid, grown at 37 °C. Complete medium required about 4 h to reach $OD_{600} \approx 0.8$, and another 4 h for optimal expression, whereas minimal medium was induced after 8−9 h and further fermented for 17−18 h. The required AMM medium was prepared by first mixing 4.5 g of KH_2PO_4, 10.5 g of K_2HPO_4, and 0.5 g of sodium citrate in 1 L of ddH_2O, and then after autoclaving, 1 mL of 1 M $MgSO_4$, 0.5 mL of 100 mg/mL ampicillin, 12.5 mL of 24 g/100 mL of glucose, 6.2 mL of 16 g/100 mL of ammonium chloride (^{14}N or ^{15}N), and 6 mL of bacterial cultures grown overnight in LB + ampicillin were added. Both conditions afforded approximately 4 mg of hHO per liter of culture. The protein was purified as reported before, the activity was measured using the bilirubin assay, and the heme content was estimated from the Soret absorbance.[40] Finally, the enzyme was inhibited by cyanide (10 molar equiv of KCN) before concentration to less than 2 mL of 1−2 mM of 1:1 heme:labeled-hHO (PH = protoheme, R = vinyl in Figure 1) complex, designated [^{15}N]-hHO−PH−CN, in 100 mM KPi at pH 7.4.

NMR Spectroscopy. ^{1}H and ^{15}N NMR data sets were collected on a Bruker AVANCE 600 spectrometer operating at 600 and 60.9 MHz, respectively. ^{1}H chemical shifts are referenced to 2,2-dimethyl-2-silapentane-5-sulfonate, DSS, through the water resonance calibrated at each temperature. ^{15}N chemical shifts are indirectly referenced from the proton spectrum.[41] Unless otherwise stated for proton spectra, the water frequency was centered on the carrier and the repetition rate was 1s^{-1}. ^{15}N-decoupled proton spectra were acquired with GARP decoupling[42] during acquisition over a bandwidth of ~200 ppm (12 kHz) centered at 110 ppm in the ^{15}N spectrum. Using a standard Bruker pulse sequence, ^{15}N 90° pulse widths were indirectly determined from the proton spectra by adjusting the ^{15}N pulse width so that the intensity of signals from protons directly attached to ^{15}N is null; the ^{15}N 180° pulse was taken as twice the 90° pulse. One-dimensional (1D), ^{15}N-decoupled and nondecoupled proton reference spectra were acquired using a standard one-pulse sequence with saturation of the water solvent signal or using a "soft" "3-9-19" pulse sequence[43,44] for water suppression.^{1}H WEFT-spectra[45] were recorded at a repetition rate of 6 s^{-1} and a relaxation delay of 50 ms. NMR data were processed using Bruker XwinNMR 3.1 or Felix on an SGI workstation. 1D spectra were zero filled to 4096 data points and apodized using an exponential function with a line broadening of 5 Hz prior to Fourier transformation.

1D ^{15}N filtered "3-9-19" proton spectra were acquired by inserting an X-half filter[46,47] immediately before a "3-9-19" pulse. Steady-state nuclear Overhauser effect (NOE) difference spectra were recorded by application of a low-powered presaturation pulse on the H_2O signal prior to the ^{15}N filter; the H_2O signal was saturated to approximately 80% of its original intensity (determined from a detuned probe). Off-resonance spectra were collected to provide a reference. To suppress

(39) Wilks, A.; Black, S. M.; Miller, W. L.; Ortiz de Montellano, P. R. *Biochemistry* **1995**, *34*, 4421−4427.

(40) Wilks, A.; Demontellano, P. R. O. *J. Biol. Chem.* **1993**, *268*, 22357−22362.
(41) Wishart, D. S.; Bigam, C. G.; Yao, J.; Abildgaard, F.; Dyson, H. J.; Oldfield, E.; Markley, J. L.; Sykes, B. D. *J. Biomol. NMR* **1995**, *6*, 135−140.
(42) Shaka, A. J.; Barker, P. B.; Freeman, R. *J. Magn. Reson.* **1985**, *64*, 547−553.
(43) Piotto, M.; Sandek, V.; Sklenar, V. *J. Biomol. NMR* **1992**, *2*, 661−666.
(44) Sklenar, V.; Piotto, M.; Leppik, R.; Saudek, V. *J. Magn. Reson., Ser. A* **1993**, *102*, 241−245.
(45) Gupta, R. K. *J. Magn. Reson.* **1976**, *24*, 461−465.
(46) Neuhaus, D.; Wagner, G.; Vasak, M.; Kagi, J. H.; Wuthrich, K. *Eur. J. Biochem.* **1984**, *143*, 659−667.
(47) Kogler, H.; Sörenson, O. W.; Bodenhausen, G.; Ernst, R. R. *J. Magn. Reson.* **1983**, *55*, 157−163.

artifacts, recording of on- and off-resonance FIDs were interleaving and stored separately. The computer difference spectra from coadding the on-resonance FIDs and coadding the off-resonance FIDs generate the fractional intensity change.

Phase-sensitive, 2D ^{15}N decoupled ^1H–^1H NOESY spectra (40 ms mixing time) were recorded either with presaturation or with a "3:9: 19" pulse for water suppression. ^{15}N decoupling, in the indirect dimension, was achieved by placing an ^{15}N 180° pulse in the center of the t_1 incremental delay and, in the observe dimension, by GARP[42] decoupling during acquisition. F1/F2 ^{15}N-filtered NOESY spectra were acquired by inserting the filter sequence before the t_1 incremental delay for the indirect dimension and prior to acquisition for the direct dimension. 2048 × 512 complex points were collected over 30 h. The acquired 2048 × 512 data were apodized with a 60°-shifted sine-squared-bell window function in both dimensions and zero-filled to give a final matrix of 2048 × 2048 points prior to Fourier transformation. Two-dimensional TPPI ^1H–^{15}N heteronuclear, single-quantum correlation (HSQC)[48] and echo/antiecho transverse relaxation-optimized (TROSY)[49] spectra were acquired with a "3-9-19" pulse for water suppression. The ^{15}N dimension was acquired with 512 increments covering a sweep width of 62 ppm; in the acquisition ^1H dimension, 2048 data points were collected. Spectra were apodized with a 30°-(^1H)- and 45°-(^{15}N)-shifted sine-squared-bell window function and were zero-filled to give a final matrix of 2048 × 1024 points prior to Fourier transformation.

3D {^1H–^{15}N}–^1H HSQC-NOESY[50] (40 ms mixing time) and 3D {^1H–^{15}N}–^1H HSQC-TOCSY[51,52] (20 ms mixing time) spectra were acquired at 30 °C with 2048 × 64 × 192 complex points that span sweep widths of 11 × 50 × 11 ppm. Data sets were linear-predicted[53] to twice the number of points in both indirect dimensions, apodized with 80°-, 80°-, and 90°-shifted sine-bell-squared window functions and zero-filled to give a final 3D data set of 2048 × 128 × 512 points prior to Fourier transformation. Phase-sensitivity for the HSQC-NOESY spectra was achieved using the States-TPPI[54] method in both dimensions and for the HSQC-TOCSY using TPPI for the NOESY and echo– anti-echo for the HSQC dimension. The MLEV 17[55] sequence was used the spin-lock for the TOCSY. Processing and analysis of the 3D NMR data sets were carried out using Felix software.

Results

The earlier study of NOEs from localized water molecules to slowly exchanging labile protons involved in strong H-bonds was carried out on hHO-DMDH–CN[34] (DMDH with R = CH$_3$ in Figure 1). This complex was investigated because it was homogeneous and exhibited narrower ^1H NMR lines than hHO– PH–CN and, hence, permitted a more definitive 2D ^1H characterization[25] than for the PH (R = vinyl in Figure 1) complex.[24] Since the ^{15}N-labeled hHO is available solely as the [^{15}N]-hHO–PH–CN complex,[56] we pursue, in parallel, in this work NMR studies on both [^{15}N]-hHO–PH–CN and unlabeled hHO–DMDH–CN. The ^{15}N chemical shifts (together with the other backbone ^1H signals for the hHO–PH–CN complex) are listed in Table 1, and the presently assigned side chain proton

chemical shifts for [N^{15}]-hHO–PH–CN and hHO–DMDH– CN are provided in the Supporting Information. The parallel investigation of the complexes with the alternate hemins has the added benefit of demonstrating that all signals near the heme displayed detectable and often significant chemical shift differences for the two hemins, while the signals for residues more remote from the substrate, such as many of the residues in the H-bond network, exhibited essentially indistinguishable shifts for the alternate substrates. The resolved, low-field portion of the 600 MHz ^1H NMR "3:9:19" reference spectrum[43] of hHO– PH–CN at 30 °C is compared to the "3:9:19" spectrum of hHO–DMDH–CN in Figure 2A and C, respectively. Resonances are labeled as assigned previously[25] or as determined in the present work. The close similarity of chemical shifts for the homologous protons in the two complexes is apparent.

At lower temperatures, a previously undetected labile proton is observed (labeled *a* in Figure 2E) in the low-field window of hHO–DMDH–CN that is suppressed by magnetization transfer[57] due to chemical exchange at elevated temperature. A similar peak appears for hHO–PH–CN (not shown), but the multiple peaks due to the heme orientational isomerism[23,24] make its detection difficult even at 10 °C. WEFT spectra[45] (not shown) for hHO–DMDH–CN at 10 °C show that peak *a* exhibits very strong ($T_1 < 50$ ms) paramagnetic relaxation. The chemical shift, relaxation behavior, and exchange saturation-transfer properties[58] are suggestive of the ring N$_\delta$H of the ligated axial His25, and the peak is tentatively identified as such.

To describe the position of assigned residues in the hHO– PH–CN complex, we adopt the description for the eight helices A–H (and the pertinent residues)[15,59] of mammalian HO as follows: A or proximal (Asp12–Ala31), B (Ala31–Lys39), C (Thr43–Lys69), D (Arg85–Gly98), E (Thr108–Glu125), F or distal (Leu128–Asp156), G (Ser174–Leu189), and H (Thr192– Leu221) helices. Four loops that resemble single-turn helices are two CD loops (Phe74–Tyr78 and Phe79–His84), a DE loop (Arg100–Val104), and an FG loop (Leu164–Thr168). The six fragments, previously labeled I–VI, whose residues have been identified[25] correspond to parts of helix A(I), helix F(II), helix D(III and VI), loop FG(IV), and helix C(V).

^{15}**N Heteronuclear Correlation.** The 30 °C, pH 7.4, {^1H– ^{15}N}HSQC spectrum[48] of [^{15}N]-hHO–PH–CN is illustrated in Figure 3; close to 300 cross-peaks are detected. TROSY spectra[49] did not lead to detectable line narrowing and failed to resolve any additional peaks. Assigned cross-peaks are labeled by residue number for peptide NHs and by residue number and position for side chain NHs. The identity of the numerous assigned peaks in the crowded panel E are labeled in an expanded spectrum in the Supporting Information. The clearly detected 23 (of the 25 Gln, Asn) NH$_2$ pairs, 9 likely Arg N$_\epsilon$H

(48) Andersson, P.; Gsell, B.; Wipf, B.; Senn, H.; Otting, G. *J. Biomol. NMR* **1998**, *11*, 279–288.
(49) Pervusin, K.; Riek, R.; Wider, G.; Wuthrich, K. *Proc. Natl. Acad. Sci. U.S.A.* **1997**, *94*, 12366–12371.
(50) Talluri, S.; Wagner, G. *J. Magn. Reson., Ser. B* **1996**, *112*, 200–205.
(51) Vuister; Bax, A. *J. Magn. Reson.* **1992**, *98*, 428–435.
(52) Schleucher, J.; Schwendinger, M.; Sattler, M.; Schmidt, P.; Schedletzky, O.; Glaser, S. J.; Sorensen, O. W.; Griesinger, C. *J. Biol. NMR* **1994**, *4*, 301–306.
(53) Barkhuisjen, H.; deBeer, R.; Bovee, W. M. M. J.; van Ormondt, D. *J. Magn. Reson.* **1985**, *61*, 465–481.
(54) Marion, D.; Ikura, M.; Tschudin, R.; Bax, A. *J. Magn. Reson.* **1989**, *85*, 393–399.
(55) Bax, A.; Davis, D. G. *J. Magn. Reson.* **1985**, *65*, 355–360.
(56) TOCSY spectra exhibited significantly more cross-peaks for hHO– DMDH–CN than hHO–PH–CN.[25] However, the discovery that the symmetric heme, DMDH, yields not only the expected single species with respect to heme orientation disorder[23,24] but also exhibited narrower lines due to faster interconversion of the dynamic structural heterogeneity was made at the same times as the [15N]-hHO and its PH complex was being prepared. At this time, an effective and quantitative route, without unacceptable losses, to replacing PH with DMDH in the pocket of the [2015N]hHO–PH–CN sample has not been designed but is under study.
(57) Sandström, J. *Dynamic NMR Spectroscopy*; Academic Press: New York, 1982.
(58) La Mar, G. N.; Satterlee, J. D.; de Ropp, J. S. In *The Porphyrins Handbook*; Kadish, K. M., Smith, K. M., Guilard, R., Eds.; Academic Press: San Diego, 1999; Vol. 5, pp 185–298.
(59) Sugishima, M.; Sakamoto, H.; Kakuta, Y.; Omata, Y.; Hayashi, S.; Noguchi, M.; Fukuyama, K. *Biochemistry* **2002**, *41*, 7293–7300.

Table 1. ¹⁵N−¹H and Cα¹H Chemical Shifts for Assigned Residues in [¹⁵N]-hHO−PH−CN

residue	Cα¹H[a]	N¹H[a]	¹⁵N[b]	δ$_{dip}$(¹⁵N)[c]	residue	Cα¹H[a]	N¹H[a]	¹⁵N[b]	δ$_{dip}$(¹⁵N)[c]
Ala20	4.42	8.57	118.6	0.71	Thr108	4.06	8.12	117.5	−0.1
Thr21	4.57	7.93	103.4	1.1	Ala110	3.85	10.23	120.5	−0.1
Lys22	6.09	7.85	124.8	2.1	Met111	3.8	7.19	117.9	−0.2
Lys23	4.74	8.94	119.7	1.6	Gln112	3.71	7.85	117.9	−0.1
Glu24	4.14	8.66	116.6	1.1	Arg113	3.47	9.01	117.4	−0.1
His25	4.16	9.94	125.6	2.4	Tyr114	d	7.48	110.0	−0.2
Thr26	4.95	9.57	118.2	2.6	Arg117		(8.99)	(85.2)	(−0.2)
Glu27	3.58	7.89	120.9	0.5	His132	d	(14.52)	(172.9)	(−0.3)
Ala28	2.21	7.12	122.5	−0.8	Ala133	4.2	7.38	122.9	−0.3
Glu29	1.14	5.83	111.6	−1.7	Tyr134	3.67	8.39	117.4	−0.4
Asn30	3.92	6.21	110.8	−0.6	Thr135	2.65	6.74	111.2	−0.9
Ala31	3.81	6.19	125.6	−0.6	Asn136	3.4	6.52(9.56)	112.3(77.6)	−0.8(0.0)
Glu32	3.93	8.57	125.8	−0.4	Tyr137	5.04	8.29	117.4	−0.1
Phe33	3.85	6.62	113.7	−0.4	Leu138	2.98	6.99	112.3	−0.4
Met34	3.8	9.18	116.6	−0.6	Gly139	d	5.84	109.6	−1.1
Arg35	4.05	8.56	125.8	−0.5	Asp140	3.92	9.52	130.3	3.2
Gln38		(5.81,6.09)	(109.7)	−0.9	Leu141	3.83	6.90	113.1	1.7
Tyr58	3.82	9.09	117.4	0.0	Ser142	d	7.84	115.8	0.0
Val59	3.32	8.29	119.4	0.0	Gly143	7.53, 7.78	15.74	112.5	2.3
Ala60	3.87	6.88	120.5	0.0	Val146	3.75	7.78	121.3	0.8
Leu61	d	8.65	118.2	−0.1	Leu147		9.08	119.8	1.7
Val77	4.06	7.45			Gly163	3.62	8.56	108.8	0.2
Arg85	d	13.0	127.2	0.2	Leu164	5.37	7.41	117.4	0.3
Lys86	d	9.42	123.9	0.2	Ala165	3.98	12.05	136.8	0.3
Ala87	3.69	8.13	117.4	0.1	Phe166		11.56	122.6	0.4
Glu91	3.96	7.35	118.6	0.1	Phe167	4.31	7.38	118.3	0.7
Asp92	d	8.16	122.9	0.2	b[e]	4.06	10.71	122.4	
Leu93	4.56	9.12	121.7	0.2	b + 1	4.30	8.42	114.3	
Ala94	4.38	6.85	120.9	0.1	b + 2	3.87	8.12	123.9	
Phe95	4.05	7.48	120.1	0.1	b + 3		8.95	118.0	
Trp96	d	8.91(11.69)	118.2(131.6)	0.1(0.2)	c − 1	4.38	8.73	126.4	
Tyr97	d	9.30	114.0	0.1	c[e]	4.61	9.77	113.1	
Gly98		7.31	110.8	0.1	c + 1	4.10	6.96	123.3	
Trp101		(10.05)	(129.9)	0.1	c + 2		8.31	123.0	
Tyr107	5.2	8.41	119.5	0.0					

[a] Chemical shifts, in ppm, referenced to DSS, in ¹H₂O solution, 50 mM phosphate, pH 7.4 at 30 °C. [b] See ref 41. [c] Calculated dipolar shifts, in ppm at 30 °C, determined from the previously reported magnetic axes and the hHO−PH−H₂O crystal structure, with axial and rhombic anisotropies,[25] 2.4 × 10⁻⁸ m³/mol, and −0.58 × 10⁻⁸ m³/mol, respectively, and α = 270°, β = 19°, and κ = 220° in Figure 1. [d] The ¹H chemical shift cannot be determined with certainty; the same signals, however, have been identified in hHO−DMDH−CN.[25] [e] Unassigned four-member helical fragments B and C where peaks *b* (part of B) and *c* (part of C) participate in strong H-bonds.
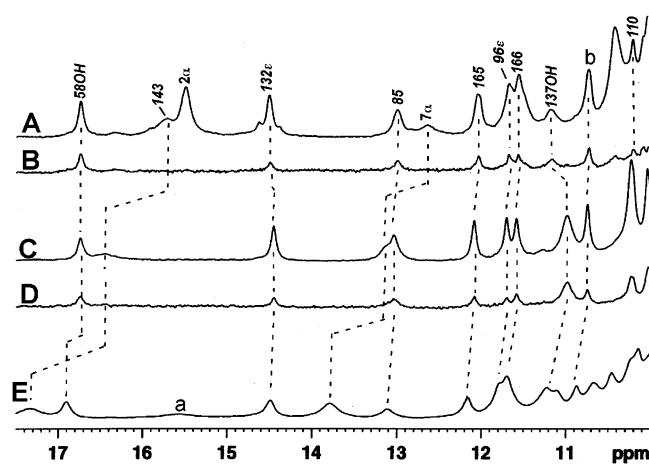

Figure 2. Low-field, resolved portions of the 600 MHz ¹H NMR "3:9:19" reference spectra in ¹H₂O at 30 °C, 100 mM in phosphate, pH 7.4 of hHO−PH−CN (A) and (C) hHO−DMDH−CN and the "3:9:19" steady-state NOE-difference traces for hHO−PH−CN (B) and hHO−DMDH−CN (D) upon saturating the water resonance. The trace of hHO−DMDH−CN at 10 °C (E) locates an additional broad, labile proton peak labeled *a* (assigned to His25 ring N$_δ$H) which is completely suppressed by extensive magnetization transfer at 25 °C. The previously and newly assigned resonances are labeled and one unassigned NH is labeled *b*.

(Figure 3B), and 1 His ring (Figure 3A) all indicate that the peptide NHs for a large fraction of the 250 nonproline residues

are detected in the {¹H−¹⁵N}HSQC spectrum at this pH. However, a significant portion of the spectrum is poorly resolved (right half portion of Figure 3E), as might be expected for an α-helical enzyme. The ¹H−¹⁵N cross-peaks to the low field of 9 ppm for ¹H (Figure 3C and E) arise primarily from previously assigned[24,25] peptide NHs for the proximal or A helix (Glu23, His25), the distal or F (Asp140) helix, and the four segments that participate in the strong H-bond network (sections III and VI on helix D, V on helix C, and IV on a loop between helices F and G). On the high-field side of the crowded window (Figure 3E) are found NHs of assigned residues with predicted[24,25] significant upfield dipolar shift (NHs of Glu29, Asn30, Ala31 (proximal helix), and Gly139 (distal helix)).

Particularly noteworthy is the observation of a weak cross-peak with peptide ¹⁵NH shift[60,61] for the 15.8 ppm broad, strongly relaxed ($T_1 ≈ 50$ ms) proton peak previously assigned[24,25] to the Gly143 NH (Figure 3C). The ¹⁵N correlation to 172.86 ppm (fold-in from the low-field side in Figure 3A) for the 14.5 ppm narrow peak previously attributed[24,34] to the His132 ring N$_ε$H confirms its assignment.[60,61] The ¹H resonance at 9.7 ppm was attributed[25] to the Arg136 N$_ε$H based on the NOE to the Tyr58 OH predicted by the crystal structure.[15]

(60) Wishart, D. S.; Bigam, C. G.; Holm, A.; Hodges, R. S.; Sykes, B. D. *J. Biomol. NMR* **1995**, *5*, 332.
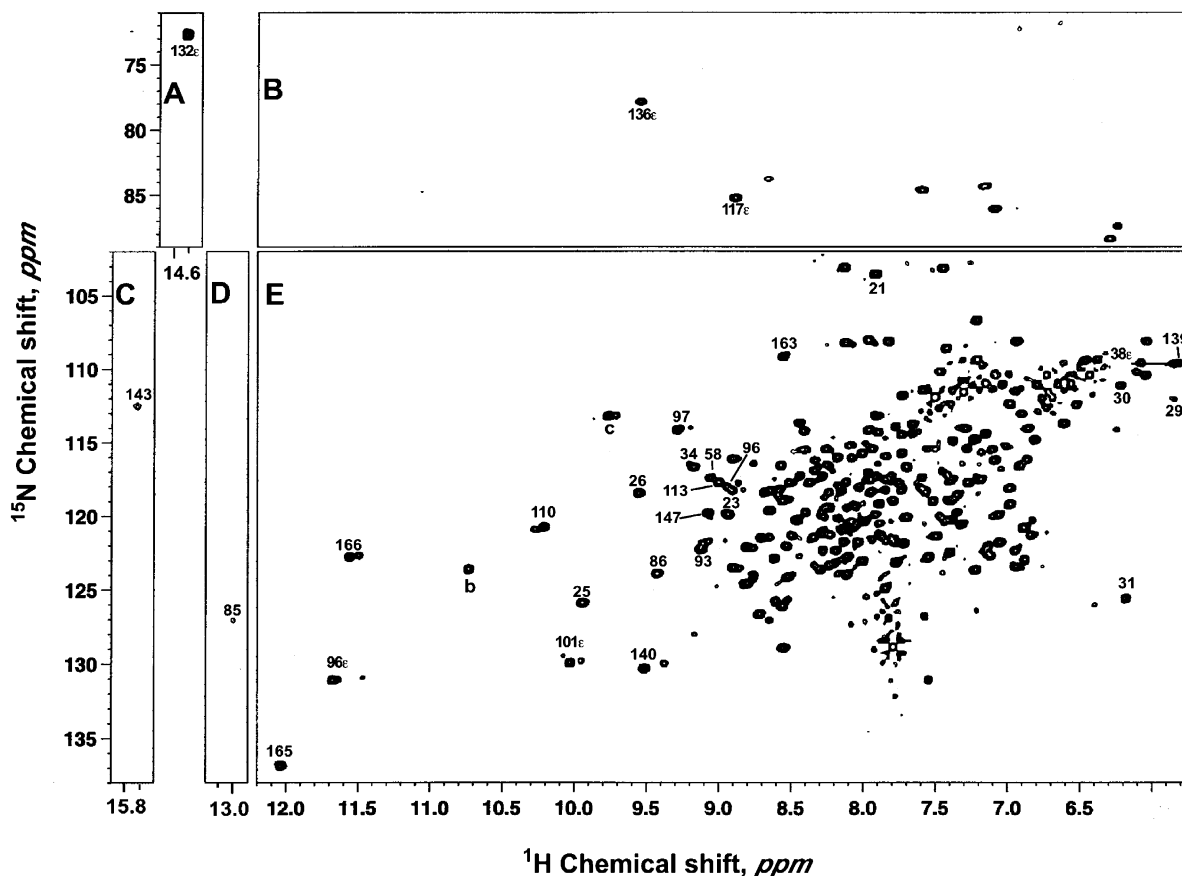(61) *BioMagResBank* (www.bmrb.wisc.edu/searchstats. diamagnetic.html).

Figure 3. 600 MHz {^{1}H$-^{15}$N}-HSQC spectrum of [^{15}N]-hHO$-$PH$-$CN in ^{1}H$_2$O, 100 mM in phosphate, pH 7.4 at 30 °C illustrating the N$-$H connections for one His side chain (A) (folded in from the low-field side at 172.8 ppm), several Arg N$_\epsilon$Hs (B), a low-field dipolar shifted peptide NH (C), and peptide NHs (D, E). The intensity of the Arg85 NH cross-peak is weak due to its proximity to the "null" in the 3:9:19 pulse. Cross-peaks of peptide NHs are identified solely by residue number, while side chain NHs are labeled by both residue number and position. It is noted that many cross-peaks to the low field of 9 ppm exhibit a smaller, nearby peak which can be traced to the alternate orientation of protohemin.[23,24] The assigned cross-peak in the crowded section E is labeled in Supporting Information.

Another labile proton at 9.0 ppm exhibits a moderate intensity cross-peak to the labile N$_\epsilon$H of His132. The crystal structure[15] predicts this proton to originate from the Arg117 N$_\epsilon$H. The correlation of these two protons to the ^{15}N spectral range[60,61] characteristic for this functionality (Figure 3B) confirm the proposed[25] Arg136 N$_\epsilon$H to Tyr58 O$_\eta$ H-bond and establishes the presence of the Arg117 N$_\epsilon$H to Glu202 carboxylate H-bond. Numerous ^{1}H$-^{15}$N correlations involving amide side chains are observed in Figure 3E, one of which corresponds to the Glu38 N$_\epsilon$H$_2$ in contact with 3-CH$_3$, as previously assigned[24,25] on the basis of the crystal structure. The ^{15}N chemical shifts for assigned residues are listed in Table 1, where we also include the N^{1}H and C$_\alpha ^1$H shifts.

Sequential Assignments. The analysis of the NOESY/ TOCSY and {^{1}H$-^{15}$N}HSQC-NOESY/TOCSY spectra[50$-$52] leads to the assignment of the backbones of the proximal or A helix from Ala20 through Asn30, which extends the assignments of this helix by 3 residues over that achieved by ^{1}H 2D NMR alone.[25] The ^{15}NH, N^{1}H, and C$_\alpha ^1$H shifts are listed in Table 1; the schematic depiction of the observed backbone dipolar connections and side chain proton chemical shifts is provided in the Supporting Information. Backbone connections among a series of TOCSY-detected NHC$_\alpha$H fragments, together with weak NOESY cross-peaks between two of the NHs and the heme 3-CH$_3$ and to an aromatic ring, extend the assignments toward the C-terminus to include helix B through Arg35 (not

shown; see Supporting Information). The C$_\alpha ^1$H peaks for the Ala31$-$Arg35 portion move upfield at lower temperature (not shown), consistent with the predicted weak to moderate upfield dipolar shifts (see Supporting Information).[25] Analysis of the two 3D maps starting with the strongly low-field (Asp140) and high-field (Gly139) assigned NHs for the distal or F helix and the previously assigned side chains[24,25] leads to the backbone for the residues Ala133 (and to His132 in hHO$-$DMDH$-$CN) to Gly143 and Val146$-$Leu147; the key sequential dipolar contacts[62] are summarized in the Supporting Information, and the backbone chemical shifts are listed in Table 1. It was not possible to locate the signals for the elusive Gly144 and Val145 near the distal helix "hinge". The relevant 3D data for helix B residues are given in the Supporting Information.

The backbones for the four previously assigned fragments (labeled III$-$VI[25]) were located in the 2D/3D data to yield the ^{15}N shifts for Arg85 to Ala88 (fragment IV) and Gln91$-$Gly98 (fragment III) on helix D, Gly163 to Phe167 on a loop between helices F and G (fragment IV), and Tyr58$-$Leu61 on helix C (fragment VI). The assignments for these fragments could not be extended over those available solely through ^{1}H 2D data, because of insufficient TOCSY cross-peaks and spectral conges- tion precluded more extensive assignments at this time. While the backbone of Ile57 could not be located in either the 2D or

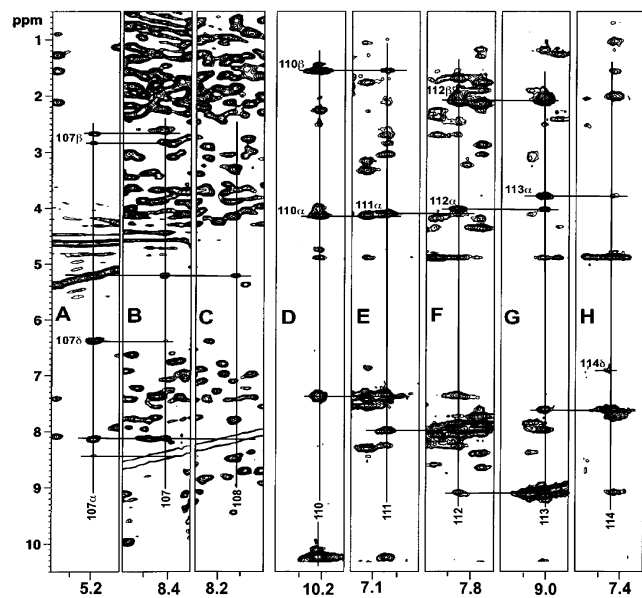(62) Wüthrich, K. *NMR of Proteins and Nucleic Acids*; Wiley & Sons: New York, 1986.

Figure 4. Sequential backbone NOESY cross-peaks for residue Tyr107−Tyr114 in [^{15}N]-hHO−PH−CN in ^{1}H$_2$O, pH 7.1 at 30 °C, as observed in portions of the F1/F2-^{15}N-decoupled NOESY spectrum for Tyr107 (A) and Thr108 (B, C) and in planes of the 3D {^{1}H−^{15}N}HSQC-NOESY spectrum for Ala110 (D) (^{15}N at 120.54 ppm) for Met111 (E) (^{15}N at 117.92 ppm), Gln112 (F) (^{15}N at 117.8 ppm), Asn113 (G) (^{15}N at 117.42 ppm), and Tyr114 (H) (^{15}N at 109.99 ppm). The mixing time in each case is 40 ms.

3D spectra, a TOCSY detected CH$_3$−CH−CH with a very large upfield bias for the resolved methyl group with a temperature independent shift at −0.3 ppm exhibits the dipolar contacts to the Tyr58 ring and backbone that is unique for the Ile57 C$_\gamma$H$_3$ group. The backbone of the key Glu62 that provides the acceptor to the strong H-bond by Arg85 could not be located in the 2D or 3D data for [^{15}N]-hHO−DMDH−CN, even though this residue has been assigned by 2D ^{1}H NMR alone in hHO−DMDH−CN.[25] Dipolar contacts for new assignments are summarized in the Supporting Information, and the backbone ^{1}H and ^{15}N shifts are listed in Table 1.

Three peptide NHs with chemical shifts > 9 ppm remain unassigned at this stage. Since they exhibit negligible paramagnetic relaxation, their low-field bias must reflect moderate to strong H-bonds.[33] A previously located,[25] but unassigned Ala with NH at 10.9 ppm, allows tracing the backbone for a six member fragment (with a backbone connection in NOESY and {^{1}H−^{15}N}HSQC−NOESY connections illustrated in Figure 4) which, together with TOCSY spectra, identify a helical fragment AMX$_i$−Thr$_{i+1}$−(α)$_{i+2}$−Ala$_{i+3}$−Z$_{i+4}$−AMX$_{i+5}$−Z$_{i+6}$−AMX$_{i+7}$ (Z long chain) with characteristic N$_i$−N$_{i+1}$, α_i−N$_{i+1}$, β_i−N$_{i+1}$, α_i−N$_{i+3}$, and/or α_i−β_{i+3} contacts[62] (not shown; see Supporting Information). Spin system AMX$_i$ and AMX$_{i+7}$ each exhibit NOESY contact to two-spin aromatic rings (one previously assigned[25] to Tyr114). The sequence uniquely identifies this fragment as Tyr107−Tyr114, part of helix E, with the strong low-field bias NH for Ala110 indicative of a strong H-bond. The Thr108 O$_\gamma$H exhibits a similarly low-field biased resonance position for the residue[61] (compare to 5.8 ppm for Thr21 in hHO−DMDH−CN[25]) indicating that it also is involved in a relatively robust H-bond. The crystal structure of hHO−PH−H2O identifies[15,17] the carboxylate of Glu216 on helix H as the acceptor for both the Ala110 NH and Thr108 OH donors.
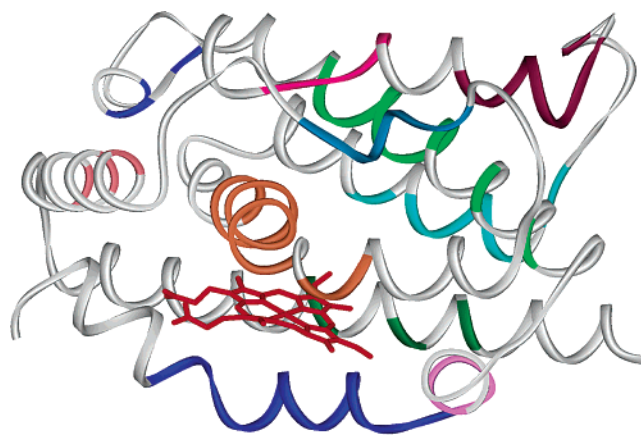

Figure 5. Ribbon structure of hHO−PH−CN depicting colored regions for which residue assignments have been carried out in hHO−PH−CN and hHO−DMDH−CN; helix A (dark blue), helix B (magenta), helix C (light green), helix D (brown), helix E (aqua), helix F (orange), helix G (light brown), and helix H (dark green); loops between C and D (blue for the first loop residues 74−78, purple for the second lop residues 79−84) and loop between helices F and G (light blue). The heme is shown in red.

The remaining two low-field NH peaks, labeled *b* (at 10.6 ppm- in Figures 2 and 3) and *c* (at 9.65 ppm in Figure 3), exhibit minimal paramagnetic influences and low-field bias indicative of moderate strength H-bonds. However, the tracing of the backbones of the two helical fragments B (including peak *b*) and C (including peak *c*) (not shown; see Supporting Information) locate two four-residue helical fragments, but neither the ^{1}H TOCSY[63] nor {^{1}H−^{15}N} HSQC-TOCSY[51,52] allowed the detection of sufficient side chain scalar connections to come up with unique assignments for either fragment. The backbone chemical shifts for fragment B and C are included at the end of Table 1, and the 3D NMR data and pattern of sequential backbone connectivities are summarized in the Supporting Information. The essentially indistinguishable chemical shifts for these fragments in the PH and DMDH complexes indicate that they are located relatively remote from the heme. The location of all assigned residues is color coded on the ribbon structure of hHO−PH−H2O in Figure 5.

^{15}N-Filtered 1D/2D Spectra. The 6 to 9 ppm spectral window of the "3:9:19" ^{1}H NMR reference spectrum[43] of ^{15}N-decoupled [^{15}N]-hHO−PH−CN in ^{1}H$_2$O is illustrated in Figure 6A, followed by the ^{15}N-filtered[43,46] "3:9:19" reference trace shown in Figure 6B (vertical expansion in Figure 6B′). The ^{15}N-filtering reduces the overall 6 to 9 ppm envelope intensity by a factor ~3−4, as expected from suppression of the NH signals (~350), and leaves the nonlabile protons for the aromatic side chains, Tyr, Thr, and Ser OHs and hyperfine shifted resonances (~120 protons), and NHs with ineffective ^{15}N-filtering due to exchange. The signals of numerous key aromatic rings (Phes 47, 166, and 167) involved in an aromatic cluster[24,25] are hopelessly lost in the normal spectrum (Figure 6A) but are clearly resolved in the ^{15}N-filtered trace (Figure 6B,B′).

The 6−9 ppm portion of the ^{15}N-filtered NOESY spectrum[46] is illustrated in Figure 6D and E and contains solely cross-peaks within and among aromatic rings and OHs to aromatic rings. The ^{15}N-filtering leads to a very significant improvement in resolution, allowing the detection of multiple interaromatic rings

(63) Griesinger, C.; Otting, G.; Wüthrich, K.; Ernst, R. R. *J. Am. Chem. Soc.* **1988**, *110*, 7870−7872.
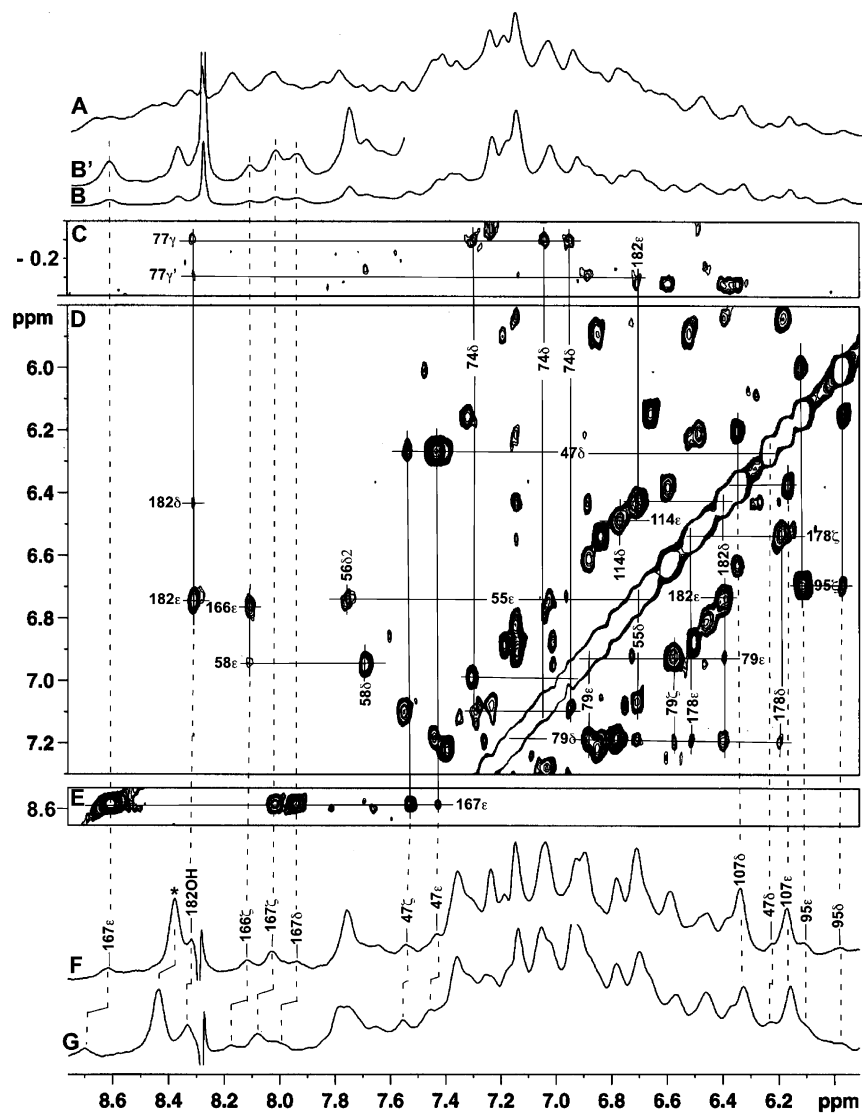
Figure 6. Window (6 to 9 ppm) of the "3:9:19" ^{1}H NMR spectrum[43] of [^{15}N]-hHO−PH−CN at 35 °C without (A) and with (B) ^{15}N-filtering,[46] which leads to a factor 3−4 reduction in intensity for the envelope; (B′) shows the vertical expression of B in the 7.5 to 9.0 ppm window, which resolves the Phe147, Phe167, and some of the Phe166 ring resonances. The ^{15}N-filtered NOESY 35 °C spectrum,[46] (40 ms mixing time) illustrating key aliphatic−aromatic (C), and intra-aromatic and interaromatic ring and hydroxyl proton (D, E) dipolar contacts, many of which are obscured in unedited NOESY spectra. The "3:9:19" steady-state NOE difference traces upon saturating water at 35 °C (F) and at 25 °C (G) illustrating the NOEs between water protons and the ring protons of Phe47, 95, 166, and 167 and Tyr107.

and OH-ring contacts, obscured in the normal NOESY spectrum.[24,25] Thus all of the expected NOESY contacts among the three rings of Phe79, Phe178, and Tyr182 and among Phe 47, Tyr58, Phe166, and Phe167 rings are easily observed (Figure 6D,E), as is the contact between the Tyr182 ring and its slowly exchanging OH (Figure 6D). The contact between the Tyr182 ring (and its OH) with an upfield-shifted TOCSY-detected (not shown) Val (Figure 6C) is consistent only with Val77. The other three-spin aromatic ring contact (Figure 6C) to Val77 can only arise from Phe74. The dipolar contact between a single, narrow signal at 7.8 ppm with minimal temperature dependence and a two-spin aromatic ring (Figure 6D) is consistent only with the expected His56 $C_\delta H$ to Tyr55 $C_\delta H$ inter-ring contacts. The proton chemical shift for these assigned residues are listed in the Supporting Information.

Dipolar Contacts with Water. Previously, it had been demonstrated[34] that the slowly exchanging backbone NHs of Ala165, Phe166, Arg85 and Lys86, and the side chain NHs of

Trp96, His132, Arg136, exhibit temperature-independent ∼10−15% negative NOEs upon saturating the bulk water signal in hHO−DMDH−CN. The size of the NOEs correlate with the solvent ^{1}H/^{2}H ratio. An eighth labile proton involved in a very strong H-bond (Tyr58 OH signal at 16.9 ppm) exhibited exchange contributions at elevated temperature, but which appeared suppressed at lower temperatures.[25,34] The "3:9:19" ^{1}H NMR spectra in Figure 2 show that water interacts in the PH complex (Figure 2A,B) with the H-bond donor protons in the H-bonding network in a fashion similar to that in the complex with DMDH[25] (Figure 2C,D). Moreover, steady-state NOE difference spectra for both hHO−PH−CN (Figure 2B) and hHO−DMDH−CN (Figure 2C) show that similar temperature-independent (not shown) NOEs from bulk water are observed for three additional labile protons whose exchange rates are too slow to contribute to the magnetization transfer. One is the presently assigned Ala110 NH at 9.92 ppm, and the other two are, as yet, unassigned peptide NHs at 10.30 ppm

(peak *b*) and 9.65 ppm (peak *c*) (not shown), both of which exhibit negligible paramagnetic influences and chemical shifts indicative of forming strong H-bonds.

The ^{15}N-filtered "3:9:19" NOE difference trace for the 6−9 ppm spectral window, upon saturating the bulk water signal, is shown in Figure 6F, which reveals temperature-independent ∼10−15% negative steady-state NOEs to all three resolved signals of Phe167, to the only resolved, low-field C$_\zeta$H of Phe166 and to all three proton signals of Phe47. Slightly stronger NOEs (∼15−20%) are observed for both ring protons of Tyr107. While the NOE to the resolved C$_\delta$H signal for Phe95 can be observed without the aid of ^{15}N-filtering,[34] we observe here NOEs to the C$_\epsilon$Hs as well. The definitive attribution of these NOEs to the previously assigned aromatic rings is evident in the steady-state NOE difference trace upon saturating water at 25 °C, as shown in Figure 6G, where the NOEs to the ring of Phe47, Phe166, and Phe167 accurately track the temperature-dependent shifts[24,25] for these low-field dipolar-shifted residues.

The magnetization transfer to two OHs in Figure 6F and G (weakly to Tyr182 OH and strongly to the peak at ∼8.4 ppm) likely arise from chemical exchange. The latter peak exhibits NOESY cross-peaks to the aliphatic spectral window and must arise from an as yet unassigned Ser or Thr side chain. While there is strong magnetization transfer between bulk water and numerous resonances in the very crowded 6−7.5 ppm window, it was not possible to unambiguously assign any of these residues, inasmuch as there are likely numerous OHs remaining in the spectral window. Further characterization of water−aromatic ring NOEs will have to rely on future studies with a ^{13}C,^{15}N-labeled sample.

Discussion

Resonance Assignments. The analysis of the 3D {^{1}H−^{15}N}-HSQC-NOESY/TOCSY data at this stage results in only a modest increase in the number (∼20) of assignments of key residues over those achieved by 2D 1H NMR alone on the hHO−DMDH−CN complex.[24,25] The present limitation this time was the inability to detect the required TOCSY peaks (in either 2D or 3D experiments in the PH complex[56]). The absence of the crucial TOCSY cross-peaks in hHO−PH−CN was noted previously and ascribed to the significant line broadening observed for many resonances due to the dynamic interconversion among at least two structures of the active site.[24,56] Two alternate configurations for the distal pocket were observed for the two nonequivalent molecules in the unit cell in the crystal structure of hHO−PH−CN.[15,17] More extensive assignments and structural characterization will be pursued in the future on a [^{15}N]-hHO−DMDH−CN complex[56] and by ^{15}N,^{13}C 3D NMR on a [^{13}C,^{15}N]-labeled hHO complex.

The new assignments, however, do confirm extremely important functionalities attributed to slowly exchanging side chain NHs, such as the N$_\epsilon$H of His132, the N$_\epsilon$Hs of Arg117 and Arg136, and the strongly relaxed, low-field labile proton at 15.7 ppm as a peptide NH of Gly143. The δ_{dip}(calcd) for the assigned ^{15}N, based on the previously reported magnetic axes[25] (given in Table 1), are generally small, and even Gly143, with the largest δ_{dip}(calcd), does not move the ^{15}N signals out of the window characteristic of peptide NHs.[60,61] The location of the presently assigned residues in the ribbon structure of hHO−PH−H$_2$O is shown by color in Figure 5. They represent
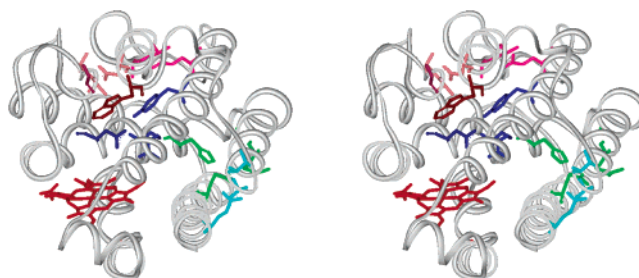

Figure 7. Stereoviews of the ribbon structure of hHO−PH−H$_2$O depicting the strong H-bond donor pairs identified by ^{1}H NMR, and the crystallographically identified acceptors. The donor→acceptor pairs are Tyr58 OH → Asp140 CO$_2^-$/Arg136 N$_\epsilon$H → Asp140 CO$_2^-$ (dark blue), Ala165 NH → Glu62 CO$_2^-$/Phe166 NH → Asp92 CO$_2^-$ (pink), Arg85 NH → Asp92 CO$_2^-$/Lys86 NH → Glu62 CO$_2^-$ (magenta), Typ96 N$_\epsilon$H → Gly163 C=O (brown), His132 N$_\epsilon$H → Glu202 CO$_2^-$ (green)/Arg117 N$_\epsilon$H → Glu202 CO$_2^-$ (light blue), and Ala110 NH → Glu216 CO$_2^-$/Thr108 OH → Glu216 CO$_2^-$ (aqua). The heme is shown in red. It is noteworthy that the strong H-bonds are largely among different secondary structural elements that exclude only the proximal A, B helices.

assignments of only ∼30% of the total residues, but they are clustered in the mechanistically important substrate binding pocket, the H-bonding network, and the aromatic cluster on the distal side (see below). Moreover, the assigned residues involve a large number of tertiary contacts among the various helices and loops. The retention or loss of these specific tertiary contacts will be invaluable in assessing the nature of the structure of hHO upon removal of the substrate.[17,59] Such ^{1}H NMR studies of apo-hHO are in progress.[64]

H-Bonding Network. Eight strong H-bonds (NH, OH chemical shifts 10−17 ppm) in the distal side have been identified in hHO−DMDH−CN[25] and the labile proton donor, with the exception of the Tyr58 OH, shown to exhibit slow exchange (half-life >10 min) with solvent.[34] The same signals, with essentially the same chemical shifts, and hence H-bond strength, are observed in hHO−PH−CN, as shown in Figure 2A and C. We extend here the H-bond network to include the Ala110 NH whose 10.2 chemical shift for the peptide NH (with negligible δ_{dip}(calcd); see Table 1) and slow exchange rate (half-life >10 min) dictate a strong H-bond. The crystal structure[15,17] identifies the likely acceptor as the carboxylate of Glu216. The OH of the presently assigned Thr108 similarly exhibits a strong low-field bias for the functionality and argues for participation in a significant H-bond for which the crystal structure identifies the same acceptor as for the Ala110 NH, the carboxylate of Glu216. The Arg117 N$_\epsilon$H shift of 9.0 ppm is similarly indicative[65] of a robust H-bond to Glu202. Two additional peptide NHs with a strong, low-field bias (peaks *b* and *c* in Figure 3) remain unassigned at this time. The locations of the 11 identified H-bond donor and acceptor residues are shown in stereoview of the hHO fold in Figure 7. It is noted that none of the strong H-bonds involve residues on the proximal helix A. This may be significant in the context of the mammalian HO−PH−H$_2$O and apo-HO crystal structures, which showed that primarily the proximal helix is perturbed upon removing substrate.[17,18,59]

Water Molecules within the H-Bonding Network. Even ordered water molecules in an enzyme exhibit relatively rapid

(64) Li, Y.; Syvitski, R. T.; Auclair, K.; Ortiz de Montellano, P. R.; La Mar, G. N. Manuscript in preparation.
(65) Gross, K.-H.; Kalbitzer, H. R. *J. Magn. Reson.* **1988**, *76*, 87−99.

exchange ($> \sim 10^3$ s^{-1} with bulk water), such that only an averaged water signal is observed.[35] However, NOEs between the bulk water and enzyme protons can be unambiguously attributed to NOEs between the enzyme residue and a water molecule within the enzyme if the presence of other fast-exchanging, nearby labile enzyme protons can be excluded. The sign of the NOE indicates whether the water molecule tumbles faster (positive NOE) or slower (negative NOE) than the Larmor frequency[35] ($\sim 3 \times 10^9$ s^{-1} at 600 MHz). Ordered water molecules (negative NOEs) have been detected by ^{1}H NMR primarily in smaller proteins[35] and for only one hemoprotein, cytochrome c,[66,67] although functionally relevant water molecules are detected in the crystal structures of numerous heme proteins.[36]

Saturation of the bulk water signal in hHO–DMDH–CN has been shown[34] to lead to $\sim$10–15% negative NOEs to the proton donors of the eight previously assigned[32] strong H-bonds, the NHs of Arg85, Lys86, Ala165, and Phe166, and the side chain labile protons of Trp96, His132, Arg136, and Tyr58. The same signals exhibit similar NOEs to water in hHO–PH–CN (compare Figure 2B and D). The negative sign dictates the water is immobilized; the 10–15% NOEs, together with uniform $\sim$25 $\pm$ 10 ms selective relaxation rates for the resolved NHs, allowed estimates of $\sim$3 Å for the water proton–enzyme NH/OH separation.[34] The data in Figure 2A and B show that the same signals exhibit similar NOEs in hHO–PH–CN, illustrating the ordered water molecules are not sensitive to the nature of the heme substrate. Moreover, a similar magnitude NOE to the slowly exchanging NH of Ala110 locates one additional water molecule in both complexes.

Inspection of the most recent refinement of the hHO–PH–H$_2$O crystal structure[17] locates several water molecules which are sufficiently close to our assigned H-bond donors to account for the NOEs (i.e., water O atom within 4 Å of the assigned NH), as listed in Table 2. The positions of the water molecules closest to the NHs are shown in the stereoviews in Figure 8, where the water molecules are numbered as identified in the crystal coordinates.[17] The water molecules in the crystal structure, and their distances to the relevant NH/OH, are listed in Table 2. In six of the nine cases, the crystal structure identifies ordered water molecules that are consistent with resulting in the observed NOEs, with exception of the NH of Phe166, N$_\epsilon$H of Trp96, and N$_\epsilon$H of His132. However, in all three of the latter cases, the crystal structure exhibits sufficient space nearby to accommodate the additional water molecules (for water near Trp96, see next section). We therefore propose ordered water molecules A, B, and C, located near Phe166 NH, the Trp96 N$_\epsilon$H, and His132 N$_\epsilon$H, respectively, as shown in Figure 8.

Water Molecules within the Aromatic Cluster. The rings of Phe47, 95, 166, and 167, Tyr58, and Trp96 interact,[15,17,23–25] with particularly close interaction of Phe166 with Tyr58 and Phe167 with Phe47. The ^{15}N-filtered, steady-state NOEs in Figure 6 show that water exhibits 10–15% negative NOEs to all of the resolved protons of Phe 47, 95, 166, 169 (but not to Trp101), as well as $\sim$20% negative NOEs to the ring protons of Tyr107; the ring protons for Tyr58 and the other ring proton of Trp96 are lost, and its envelope is dominated by exchange magnetization transfer to OHs in the crowded 6.5 to 7.5 ppm

(66) Qi, P. X.; Beckman, R. A.; Wand, A. J. *Nat. Struct. Biol.* **1994**, *1*, 378–382.
(67) Bertini, I.; Ghosh, K.; Rosato, A.; Vasos, P. R. *Biochemistry* **2003**, *42*, 3457–3463.

Table 2. Positions of Water Molecules Relative to H-bond Donor NH(OH) or Aromatic Ring Protons

residue	proton	water molecule^a (r_{ij}, Å)^b
Arg85	NH	**#25**^{c} (4.6), **#44** (4.6)
Leu86	NH	**#25** (3.4), **#44** (3.6)
Ala110	NH	**#297** (3.4)
Ala165	NH	**#9** (3.3), **#64** (3.6)
Phe166	NH	**A** (3.7)
Trp96	N$_\epsilon$H	**B** (2.7)
His132	N$_\epsilon$H	**C** (3.4)
Arg136	N$_\epsilon$H	**#32** (3.7)
Phe47	C$_\delta$Hs	**D** (3.9)
	C$_\epsilon$Hs	**B** (3.6), **D** (2.1)
	C$_\zeta$H	**D** (2.6)
Phe95	C$_\delta$Hs	**#269** (3.7)
	C$_\epsilon$Hs	**#107** (3.9)
Tyr107	C$_\delta$Hs	**#396** (3.7), **#39**(3.9)
	C$_\epsilon$Hs	**#111** (2.7), **#330** (3.7)
Phe166	C$_\zeta$H	**#085** (3.9), **#114** (4.0), **#225** (4.3)
Phe167	C$_\delta$H	**#225** (3.0), **#114** (3.6), **#131** (3.6)
	C$_\epsilon$H	**#225** (3.1), **#331** (3.8)
	C$_\zeta$H	#331 (4.5), **D** (3.5)

^{a} Water molecules numbered observed in the crystal structure[17] of hHO–PH–H$_2$O. Lettered water molecules (i.e., A–D) are identified here by solution ^{1}H NOEs in [^{15}N]-hHO–PH–CN. ^{b} Distance, in Å, between the water molecule O and the protons of interest, as obtained from the crystal structure[17] (numbered water) or estimated by solution NOEs (lettered water). ^{c} Water molecules shown in bold are depicted in Figures 8–10.

spectral window. The selective T_1 for the resolved NHs were shown[34] to be consistent with $\sim$3 Å NH–water proton distances. We interpret the 10–15% negative NOEs for the ring protons as reflecting similar ($\sim$3 Å) water proton to ring proton distances. Table 2 identifies the relevant ordered water molecules in the refined hHO–PH–H$_2$O crystal structure[15,17] and lists water molecule O-atom to ring proton distances < 4 Å. The positions of the closest water molecules to the aromatic rings are shown in the stereoviews in Figure 9. It is again apparent that the majority of the water NOEs to aromatic rings are readily accounted for by the crystallographically identified[17] ordered water molecules (spheres in light blue in Figure 9), with two prominent exceptions, the NOEs to the Trp96 N$_\epsilon$H and to the whole Phe47 ring. In the case of Tyr107, the NOE to C$_\epsilon$H could arise from the rapidly exchanging OH,[35] but that to the C$_\delta$H must arise from a nearby water molecule, and the crystal structure, indeed, finds water molecules (Table 2) close to both ring positions.[15,17]

There is neither a water molecule within 6 Å of the Phe47 ring in the crystal[15,17] nor one close enough to the Trp96 N$_\epsilon$H to account for the observed NOEs. However, there are vacancies of sufficient size, one between the Phe167 ring and Val42 (identified as water molecule D in Figure 9) and one between Trp96 and Gly163 (water molecule B), whose positions relative to the Phe47 (and Phe167 C$_\zeta$H) and Trp96 rings can account for the observed NOEs, as indicated by the relative distances in Table 2. The position for water molecule B responsible for the NOE to the Trp96 N$_\epsilon$H is placed so as to also account for an NOE to the only resolved signal for the Phe95 ring.[34] Our present data therefore support the presence of the water molecules in the crystal structure near the rings observed[15,17] and propose the location of two additional ordered water molecules near the rings of Trp96 and Phe47. Those water molecules observed solely in solution for hHO–PH–CN may not be sufficiently localized, or have large enough occupancy, to be detectable in the crystal.
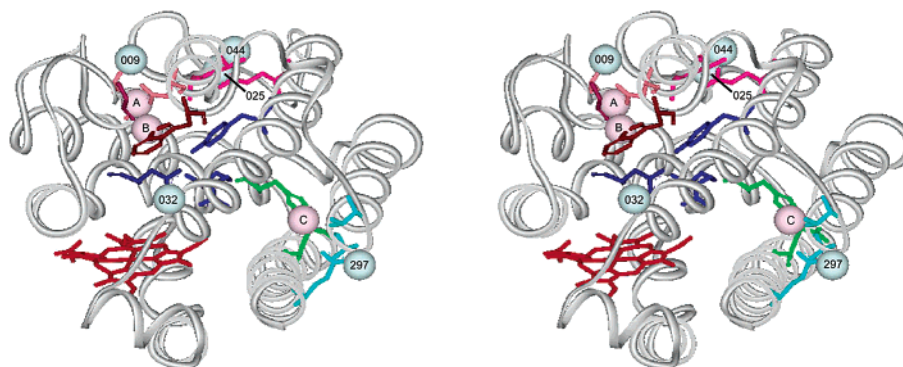
Figure 8. Stereoviews of the ribbon structure of hHO−PH−CN depicting the donor residues in the eight strong H-bonds and the NMR-identified immobilized water molecule near these donor NHs (pink and blue spheres) that account for the observed NOEs to water. The donor residue has the same color described in Figure 7. The light blue, numbered water molecules are also observed in the crystal structure[17] and are identified in Table 2. The lettered, pink water molecules labeled A−C are observed only by ^{1}H NNMR and are positioned in the available space to account for the NOEs.
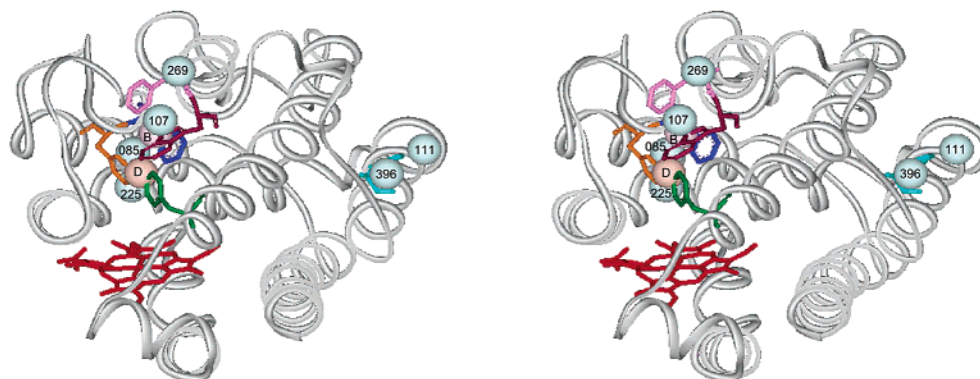

Figure 9. Stereoviews of the ribbon structure of hHO−PH−CN depicting the aromatic rings of Phe47 (green), 95 (magenta), 166 (dark blue), and 167 (orange) and Trp96 (brown) and 107 (aqua). The eight spheres represent water molecules that account for the NMR-observed dipolar contacts with the ring protons. The light blue, numbered waters are observed in the crystal structure[17](identified in Table 2), and the pink, lettered water molecules B and D are located solely by NMR.
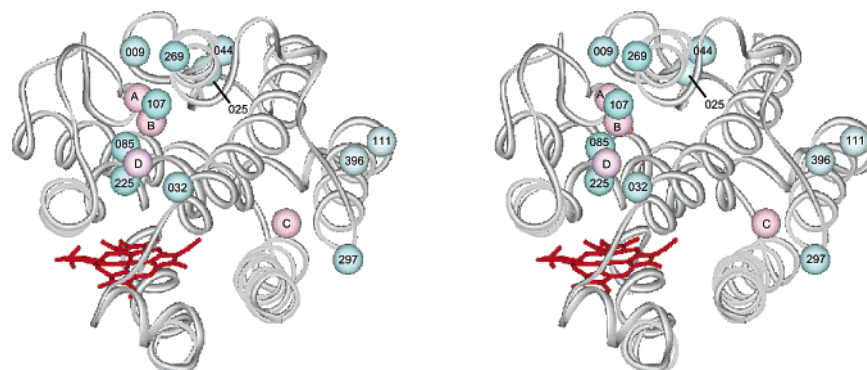

Figure 10. Stereoview of the ribbon structure of hHO−PH−H$_2$O depicting the location for the sixteen water molecules in the active site of hHO−PH−CN. The light blue spheres represents the NMR-detected water molecules which are also detected in the crystal structure[17] of hHO−PH−H$_2$O, while the pink spheres represent water molecules located only by ^{1}H NMR in hHO−PH−CN in solution. It is noted that the water molecules within the aromatic cluster complement those within the H-bonding network to form a "water channel" from the distal cavity to the enzyme surface.

Role of the H-Bonding Network and Ordered Water Molecules. The water molecules detected near H-bond donors (Figure 8), and near aromatic rings (Figure 9) complement each other so as to form a "channel" of water molecules that extends from the distal ligand to the surface of the protein on the opposite side of the substrate binding pocket, as shown in the stereoviews in Figure 10. These ordered water molecules can be envisioned to play several key roles in HO catalysis. The crystal structure of hHO−PH−H$_2$O showed that the ligated water is H-bonded to an ordered water molecule that is also a donor to the carboxylate of Asp140[16] and lead to the pro-

posal[16,31] that a water molecule provides the titratable group detected spectroscopically[27−29] and is the source of the isotope effect on the EPR spectra of the oxy-complex of the Co(II) substituted substrate complex of rHO.[30] Recent crystal studies of, initially, rHO−PH−N$_3$[19] and, more recently, reduced hHO−PH−NO[26] show clearly that there is an ordered water molecule in H-bond contact with both the distal ligand and the Asp140 carboxylate. Hence the assumption that a water molecule provides the stabilizing H-bond to bound O$_2$ is reasonable. This conclusion is reinforced by the crystal structures of the D140A−hHO−PH−H$_2$O and reduced D140A−hHO−PH−CN com-

plexes which reveal significant differences only in the distal solvent structure. These results were used to propose a detailed mechanism[26] which involves a water molecule simultaneously serving as H-bond donor to both the bound O_2 and the Asp140 carboxylate to stabilize the hydroperoxy intermediate. The mutation of Asp140 to Ala abolishes oxygenase activity.[16,31] Moreover, the formation of the catalytically active $Fe-O-OH$ species by cryoreduction is strongly retarded in the D140A mutant relative to WT HO.[14]

This ordered, catalytically critical water molecule that serves as H-bond donor to both ligand and Asp140 is not an isolated water molecule but is part of a network of water molecules in a distal channel detected by both crystallography and NMR, and many of the ordered water molecules have been shown[34] to be very close to the donors in unusually strong H-bonds that appear to accompany the ordered water molecules. The present results contribute to this evolving picture of the mechanisms of HO activation of O_2 in several ways. On one hand, we identify herein four additional strong H-bonds that appear involved in ordering the distal water molecules. In addition, we detect in solution by ^{1}H NMR NOEs not only to 12 water molecules in the distal pocket whose positions are consistent with crystallographically detected water molecules but extend the water channel by the observation of four additional ordered water molecules, two of which appear buried between aromatic rings of the hydrophobic cluster. It is expected that planned ^{13}C-edited NOEs and NOESY spectra will locate additional ordered water molecules near the numerous aromatic rings whose signals are obscured by ^{1}H spectral overlap.

The extended H-bond/ordered water network that stretches from the active site to the protein surface is likely to also play an important role in providing, in a controlled manner, the nine protons per turnover required at the active site. Similar water channels have been identified in cytochrome oxidases,[68−70] implicated in the proton transfers of those enzymes, and have been proposed for cytochrome P450.[71] By providing a directional hydrogen bond to the iron-bound peroxo species, the H-bond/ordered water network may also help to orient the distal oxygen of the peroxo ligand toward the α-meso carbon and thus contribute to the regiospecificity of the enzyme. In a more general sense, the hydrogen bond network may help to organize the active site residues, to maintain the appropriate electrostatic environment of the active site, and to tune the redox potential of the iron to match that of cytochrome P450 reductase, its electron donor partner. Functional, spectroscopic, and structural studies of mutants designed to modulate the structure and dynamic stability of the H-bond network and ordered water molecules are in progress.

Supporting Information Available: One table (assigned side chain chemical shifts) and four figures (sequential NOESY cross-peak patterns, assigned peaks in [1]H−^{15}N HSQC spectra, sequential [1]H−^{15}N HSQC-NOESY assignments for helix B, and fragments B and C (total 8 pages, print/PDF). This material is available free of charge via the Internet at http://pubs.acs.org.

JA036176T

(68) Wikström, M. *Curr. Opin. Struct. Biol.* **1998**, *8*, 480−488.
(69) Gennis, R. B. *Biochim. Biophys. Acta* **1998**, *1365*, 241−248.
(70) Svensson-Ek, M.; Abramson, J.; Larsson, G.; Törnroth, S.; Brzezinski, P.; Iwata, S. *J. Mol. Biol.* **2002**, *321*, 329−339.
(71) Oprea, T. L.; Hummer, G.; Garcia, A. E. *Proc. Natl. Acad. Sci. U.S.A.* **1997**, *94*, 2133−2138.